ELSEVIER

Materials Science and Engineering A 432 (2006) 191–201

MATERIALS SCIENCE & ENGINEERING A

www.elsevier.com/locate/msea

The mechanical response of pure iron at high strain rates under dominant shear

D. Rittel [a,*], G. Ravichandran [b], A. Venkert [c]

[a] *Faculty of Mechanical Engineering, Technion, 32000 Haifa, Israel*
[b] *Graduate Aeronautical laboratories, California Institute of Technology Pasadena, California 91125, United States*
[c] *NRCN, Beer Sheva, IL 84190, Israel*

Received 20 June 2005; accepted 31 May 2006

Abstract

The mechanical behavior and microstructure of pure iron subjected to dominant shear loading has been characterized over a wide range of strain rates. Pure iron is found to be highly strain-rate sensitive. Iron exhibits marked strain softening at $\dot{\varepsilon} \approx 8000\,s^{-1} - \sigma \approx 850$ MPa that is unexpected for the annealed material, as characterized by TEM, but is identical to that of iron preshocked at 40 GPa [G.M. Weston, J., Mater. Sc. Lett. 11 (1992) 1361]. The microstructure is found to undergo significant refinement with increasing strain rate, from large initial grains (50 μm), through dislocation cells and large twinning, and finally micro-twins and dynamically recrystallized 200 nm grains at the higher strain rates. *In situ* temperature measurements indicate the release of an external heat source, other that the thermomechanical conversion of plastic work, which is identified as dynamic recrystallization. The present results suggest the operation of the α (BCC) $\Leftrightarrow$ ε (HCP) phase transition that is known to occur during hydrostatic or shock loading at 13 GPa. The combination of the high strain-rate sensitivity and dominant shear loading conditions seem to trigger this phase transition, thus supporting recent work [K.J. Caspersen, A. Lew, M. Ortiz, M., E.A. Carter, Phys. Rev. Lett. 10 (2004) 115501] emphasizing the role of shear.

Keywords: High strain rate; Dominant shear; Iron; Martensitic phase transformation; Dynamic recrystallization

1. Introduction

The mechanical behavior of pure iron has been extensively studied in many different contexts, ranging from its rate sensitivity [1–8], deformation micromechanisms and microstructural issues [9–19], and shock physics [20–21]. These topics are often interrelated and an underlying issue is that of the allotropic α (BCC) $\Leftrightarrow$ ε (HCP) phase transition. This phase transformation, discovered by Bancroft et al. [22], is known to be totally reversible, and occurs at large (hydrostatic) pressures, starting at 13 GPa and completing around 23 GPa [23–25]. While such high pressures are not easily attainable at low strain rates (e.g. using diamond anvils), it can more easily be applied using planar shocks [20,26]. Consequently, a very large fraction of the available literature has been dedicated to the shock behavior of α-iron, including impacts at very large velocities of the order of km/s [19]. Naturally, the materials community has extensively characterized several aspects of the microstructural evolution of this material at various strain rates. One of the first problems addressed was that of the deformation micromechanisms, in terms of twinning [9,13,15,17]. A very extensive microstructural characterization was produced by Smith [11], followed by Dieter [12] and by Leslie et al. [16]. A recent review was dedicated to micro-twins and Neumann bands [19]. Unfortunately, these studies cannot be generalized to all grades of pure Fe, as it was shown that twinning is strongly affected by the material purity, as minute traces of other elements would promote twinning as opposed to an even purer grade [13]. The same problem arises for pre-strain, as the latter may also hinder twinning [15]. Therefore, the first problem that arises when establishing comparisons among various experiments relates to the starting material condition. While all authors agree on a marked microstructural refinement as a result of high-rate deformation, one central issue remains related to the very reversibility of the phase transition. In other words, one cannot identify traces of the metastable ε phase once unloading has taken place. One noticeable exception is the recent paper of Sano et al. [27], who claim having quenched some ε phase using femtosecond laser pulses. However, the characterization of the quenched phase is still preliminary, relying on

* Corresponding author. Tel.: +1 972 4829 3261; fax: +1 972 4829 5711.
E-mail address: merittel@technion.ac.il (D. Rittel).

0921-5093/$ – see front matter © 2006 Elsevier B.V. All rights reserved.
doi:10.1016/j.msea.2006.05.154

electron backscattering diffraction (EBSD), without transmission electron microscopy (TEM) work. More generally, TEM technique has not been extensively used for pure Fe as a result of its ferromagnetism that complicates the characterization.

As mentioned before, high-rate shock experiments seem to be the best technique to investigate phase transitions in this (and other materials), but as pointed out by Jones and Graham [28], the shear component that is inherent in that experiment should not be overlooked (see also direct measurements by Millett et al., [26]). Recent work has focused on the role of shear stresses in the critical pressure for phase transformation. Specifically, Von Bargen and Böehler [29] have shown that shear stresses in the pressure-transmitting medium systematically affect the transformation pressure and hysteresis loop observed upon unloading. However, shear stresses are still considered as "stray" stresses in these references. By contrast, atomistic calculations have shown the significant contribution of shear strain, event of modest magnitude, to the $\alpha \Leftrightarrow \varepsilon$ transition [30]. However, this result has not been yet supported by direct experimental evidence, mostly due to the scarcity of high strain-rate shear tests performed so far on pure Fe. Therefore, the characterization of the mechanical properties of pure iron at high strain rates cannot be dissociated from the potential phase transformation, when almost no experimental evidence is available on the role of shear. Finally, one should mention the great interest in iron and its phase transitions in the geophysics community, as iron is a major constituent of the Earth's core [31,32]. The physical properties of Fe at extreme pressures are therefore of prime interest to this community to understand basic problems related to wave propagation such as earthquakes, among others.

The present paper contains a thorough experimental characterization of the shear dominant, large strain mechanical response of pure Fe over strain rates ranging from $\dot{\varepsilon} \approx 10^{-4}$ to $10^{4}\ \mathrm{s}^{-1}$. The evolution of the microstructure is described as a function of the strain rate. The deforming gauge's temperature is monitored *in situ* throughout the high-rate experiments and is presented here. In addition to monotonous loading, jump tests are performed to probe the response of the material to a sudden change in applied strain rate. The paper is organized as follows: first, the material, specimen and experimental techniques are presented. The experimental results are described in the next section, followed by a discussion section. Conclusions of this work are drawn in the last section.

2. Experimental

2.1. Material and specimens

The material of this study is high purity (99.8%) iron, supplied as a 25.4 mm diameter rod (see composition in Table 1). As will be shown in the sequel, the material has been annealed and a typical grain size is 50 μm. Shear compression specimens (SCS—[33]) were machined from the rod. For the sake of brevity, it will be reminded that the SCS is a cylinder or parallelepiped with two 45° slots on each side (Fig. 1). As the specimen is loaded, the material in the gauge section between the two slots experiences a three-dimensional stress state with a dominant shear component [33]. The initial slot width is variable and the strain rate can be varied by altering it. One of the main advantages of this specimen is that it can be used in a seamless manner over a wide range of strain rates, from quasi-static to high-rate dynamic loading [34]. The strains and stresses can be reduced to equivalent strains and stresses in Mises' sense. The simplified relations between displacement, load, geometrical parameters and equivalent strain ($\varepsilon_{\mathrm{eq}}$) and stress ($\sigma_{\mathrm{eq}}$) are as follows:

$$\varepsilon_{\mathrm{eq}} = \frac{d}{h}; \qquad \dot{\varepsilon}_{\mathrm{eq}} = \frac{\dot{d}}{h} \tag{1}$$

$$\sigma_{\mathrm{eq}} = k_1(1 - k_2\varepsilon_{\mathrm{eq}})\frac{P}{Dt} \tag{2}$$

where d is the prescribed displacement, h the gauge height, P the applied load, D the specimen diameter, and t is the gauge thickness, as shown in Fig. 1. k_i are constants whose value were determined as in [34], by comparing SCS results with those obtained from compression cylinders. Three different gage widths were used, $w = 2.55$, 1.65 and 0.6 mm. The value of the k_i coefficients is summarized in Table 2 for each gauge width.

Table 1
Composition of the investigated α-Fe

Element	wt.%
Fe	99.8
C	0.006
Si	0.021
Mn	0.058
P	0.003
S	0.002
Cr	0.023
Ni	0.027
Mo	0.003
V	<0.0002
Wu	<0.0007
Co	0.0041
Cu	0.01
Sn	0.004
Al	0.003
Ti	0.0004
Pb	0.0002
B	0.0001
Nb	<0.0004
N	0.005

2.2. Mechanical testing

Quasi-static testing was carried out on a computer controlled MTS servo-hydraulic machine, operated under displacement control. The machine stiffness was taken into account when producing stress–strain data. High-rate constitutive behavior was

Table 2
K coefficients as a function of the gauge width w (Eqs. (1) and (2))

	$w = 2.6$ mm	$w = 1.3$ mm	$w = 0.5$ mm
K_1	1.0	1.0	1.0
K_2	0.05	0.0	0.0
K_3	1.0	0.7	0.43

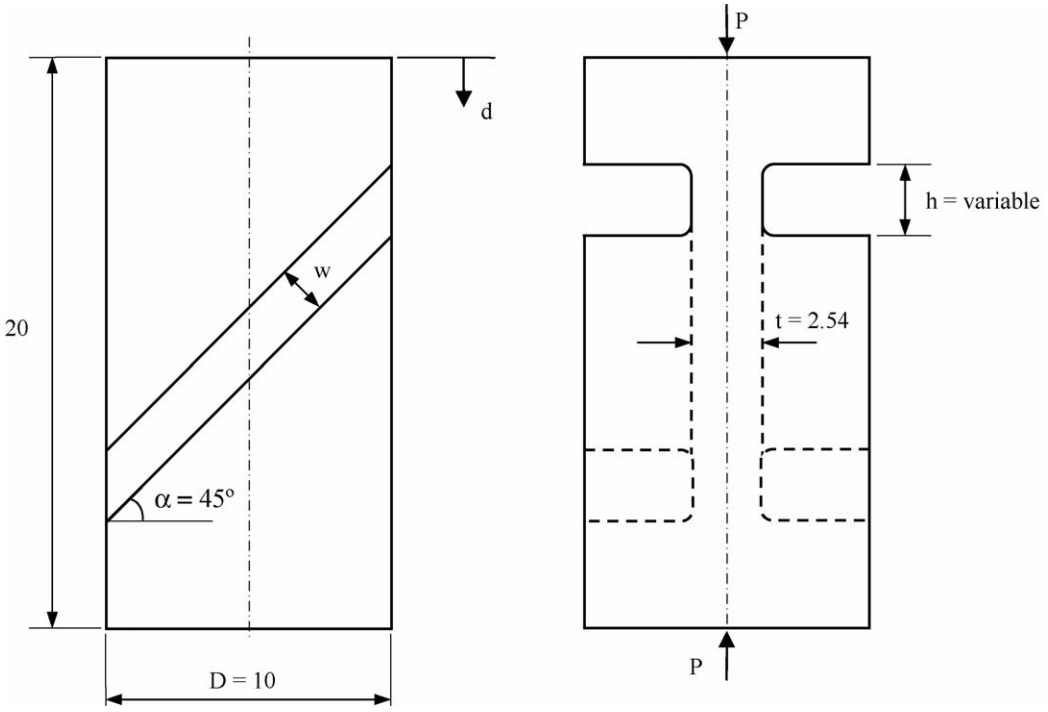

Fig. 1. Schematic representation of the shear compression specimen. All dimensions are in millimeters. *D*, *h* and *t* are the geometrical parameters used for equivalent stress and equivalent strain determination.

investigated using a 19 mm diameter Kolsky (split Hopkinson) pressure bar [35], made of C300 maraging steel. Signal processing accounted for wave dispersion according to the algorithm of Lifshitz and Leber [36]. Strain-rate jump tests were carried out using specially designed 30 cm long cylindrical projectiles. Part of the projectile had a stepwise reduced diameter. Two impacters had diameters of 19–12.7 mm and 19–9.61 mm along 15 cm each. The other set had an initial diameter of 19 mm along 8 cm and either 12.7 or 9.61 mm diameter along the remaining 22 cm. Similar projectiles were used by Nicolazo and Leroy in their study of pure iron [8].

2.3. Microstructural characterization

The microstructure of the Fe specimens was characterized using conventional optical metallographic techniques followed by transmission electron microscopy carried out in a JEOL 2000FX TEM operated at 200 kV. Samples for transmission electron microscopy were prepared from the deformed gauge section. Reference samples were taken from the undeformed parts of the specimen. The TEM samples were cut to 3 mm disks and mechanically polished to a thickness of 35 μm. The samples were finally thinned in a Gatan PIPS© ion miller. Microhardness was measured with a diamond pyramid indenter and a load of 100 g.

2.4. Temperature measurement

The evolution of the temperature in the gauge section was monitored using a single element, liquid nitrogen cooled, HgCdTe high-speed infrared detector [37]. The detector size is 1 mm × 1 mm and a Newtonian optical system with a 1:1 magnification ratio was used to gather the infrared radiation from the gauge onto the detector. While his technique is probably the best available remote sensing technique for measuring temperature, care must be exercised in order to obtain reliable a reliable conversion of the detector's voltage into temperature of the gauge. To do so, series of calibrations were performed as follows. A dummy specimen was instrumented with a thermocouple cemented at its center. The specimen was heated in a furnace and rapidly sandwiched between the two steel bars to mimic the dynamic test conditions. The thermocouple voltage was recorded simultaneously with that of the detector to obtain a correlation. Such calibrations were performed at least five times for each specimen geometry (gauge width) used in our tests. Two other factors that may influence the accuracy of the temperature determination are the loss of focus, as the specimen expands radially (for a cylinder), and the development of a gradual surface texture resulting from deformation that affects the emissivity of the gauge's surface. As result of the flatness of the SCS' gauge, the loss of focus was deemed to be minimal in these experiments. The development of a marked texture, similar to the orange-peel phenomenon in coarse-grained materials was not observed so that this factor too was not taken into account in the present experiments.

3. Results

3.1. Mechanical behavior

3.1.1. Stress–strain

Typical stress–strain curves obtained at various strain rates are shown in Fig. 2. As the strain rate increases, the apparent

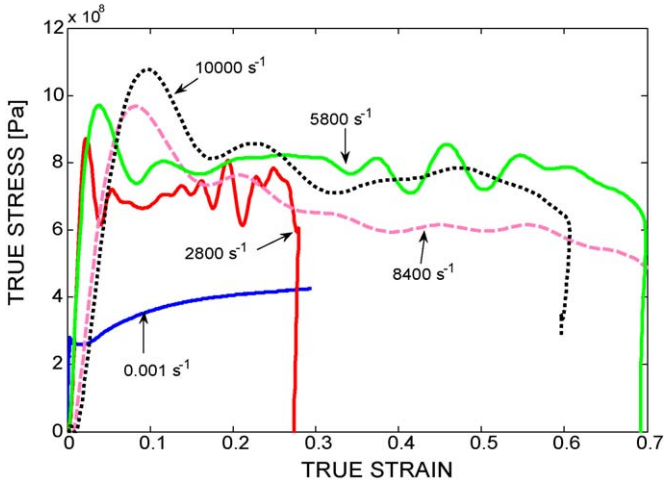

Fig. 2. True stress–strain curves at various strain rates. Note the gradual loss of hardening with increasing strain rate and the strain softening at $\dot{\varepsilon} = 8400\,\mathrm{s}^{-1}$ and beyond.

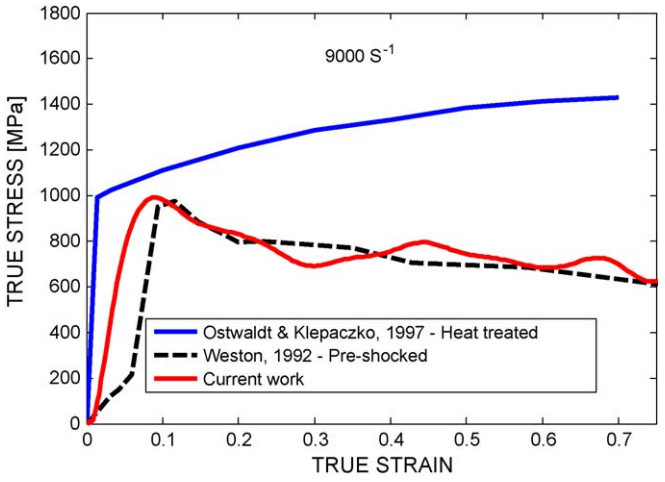

Fig. 4. Stress–strain curve at $\dot{\varepsilon} = 9000\,\mathrm{s}^{-1}$. While annealed Fe, similar to the investigated material, strain hardens at this strain rate, the present material exhibits significant softening, similar to the preshocked Fe [4].

yield stress of the material increases too, but a marked decrease in the strain-hardening capacity of the material develops gradually. Eventually at high strain rates of the order of $\dot{\varepsilon} \approx 8000\,\mathrm{s}^{-1}$, the material exhibits significant strain softening. The strong rate-sensitivity of the material can be further illustrated by plotting the stress level corresponding to a selected strain value ($\varepsilon = 0.1$ in this case) as a function of the strain rate, as shown in Fig. 3. In order to compare with previous work, experimental results from Weston [4] have been added in the figure. This author performed dynamic compression tests on pure iron cylindrical specimens that had been previously shocked to a pressure of 40 GPa, i.e. that underwent the reversible phase transformation, and also on as-received material. Fig. 3 reveals that for $\dot{\varepsilon} \leq 10^4\,\mathrm{s}^{-1}$, specimens from the present study behave like Weston's (1992) as-received material. But at higher strain rates, the strain-rate sensitivity of the investigated iron and Weston's [4] preshocked iron are quite similar. Additional insight is gained by comparing specific dynamic stress–strain curves of the present material with those of Weston [4] and of Ostwaldt et al. [5] who investigated annealed pure Fe using cylindrical specimens. As shown in Fig. 4, for the relatively high strain rate of $\dot{\varepsilon} = 9000\,\mathrm{s}^{-1}$, the Fe specimens under investigation exhibit a flow curve that is identical to that of the preshocked Fe, as opposed to the annealed material that retains its strain-hardening capacity at this strain rate.

Microhardness measurements were made across the gauge section and typical results are shown in Fig. 5. The hardness increases with the total strain reached during the experiment. A comparison of the quasi-static and high strain rate ($\dot{\varepsilon} = 11500\,\mathrm{s}^{-1}$) shows that despite the large difference in strain rates and mechanical response, the two specimens that were deformed to comparable strain levels reach similar hardness values. Therefore, for pure Fe, microhardness

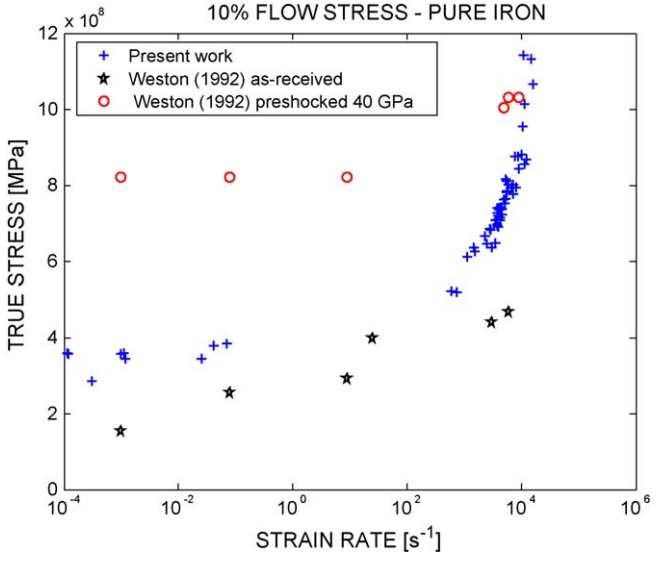

Fig. 3. Strain-rate sensitivity of the flow stress at $\varepsilon = 1$. Note the jump in behavior: for strain rates up to $\dot{\varepsilon} \approx 8000\,\mathrm{s}^{-1}$, the material behaves like Weston's [4] as-received Fe. Beyond that rate, the investigated material behaves similar to preshocked (40 GPa) Fe.

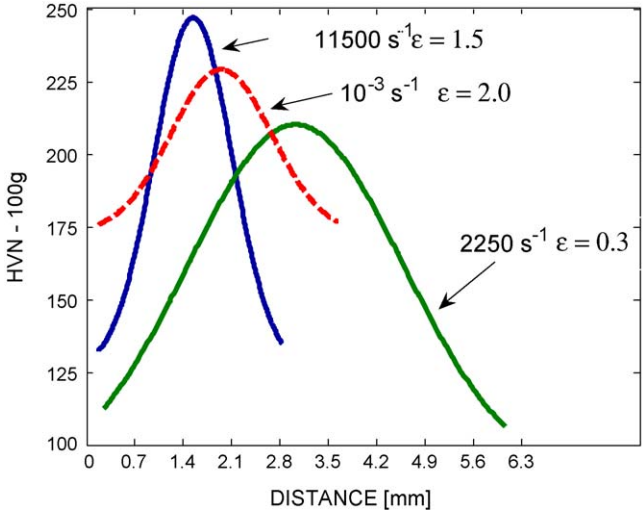

Fig. 5. Vickers microhardness values measured across the specimen's gauge. Note that quasi-static large strain deformation yields values that are similar to those obtained at high strain rate.

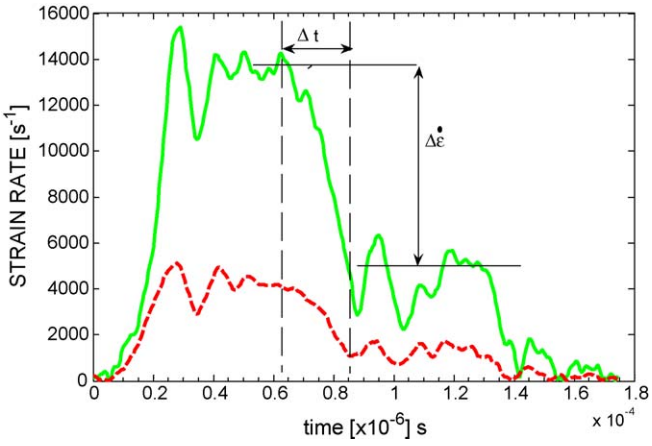

Fig. 6. Typical strain-rate signals obtained during strain-rate jump tests. The transition period lasts for $\Delta t = 27\ \mu s$ during which the strain increases.

appears to be insensitive to the loading path in terms of strain rate.

3.1.2. Strain-rate jump test

The typical strain rate varies from a constant level $\dot{\varepsilon}_1$ to the next level $\dot{\varepsilon}_2$ within a certain constant time Δt. According to the initial diameter of the impacting projectile, one can perform an ascending test in which the strain rate is increased (small followed by large diameter), or a descending test for which the strain rate is reduced, as shown in Fig. 6. It should be noted that for the fixed projectile geometry employed here, a constant time interval of $\Delta t = 27\ \mu s$ was needed for the strain rate to adjust to its next values. Only the results of descending tests are reported here. Fig. 7A shows the resulting stress–strain curve for a typical jump test. The stress–strain curves obtained from an un-interrupted test at a similar strain rate have been superimposed to assess the effect of the jump. At the higher strain-rate $\dot{\varepsilon}_1$, the two stress–strain curves are similar. However, at $\dot{\varepsilon}_2 < \dot{\varepsilon}_1$, the stress–strain curve seems to be below that of the un-interrupted tests A similar behavior has been noted by Venkadesan et al. [38] for austenitic stainless steel. These authors attributed the asymptotic stress behavior to fading memory effects, which in turn relate to metallurgical phenomena such as dynamic strain aging. Venkadesan et al. [38] addressed specifically the nature of the transient strain-rate jump, whereas this problem is usually neglected in favor of the stabilized stress–strain curves, as in [8].

The present results also reveal that the transient in applied strain rate causes a structured jump in the stress–strain curve. Fig. 7B shows the details of the stress–strain curve in the vicinity of the transition strain. Upon strain-rate reduction, the stress–strain curve oscillates as it drops rapidly below the current stress level and then rises again in an attempt to reach the new stable stress condition corresponding to $\dot{\varepsilon}_2$. One can therefore distinguish two phases: the unloading phase during which the stress decreases followed by the loading phase during which stress increases. For each phase, two instantaneous hardening moduli can be defined $M_{ij} = \left|\frac{\Delta\sigma}{\Delta\varepsilon}\right|$ for $\dot{\varepsilon}_i \leftrightarrow \dot{\varepsilon}_j$, where σ, ε and $\dot{\varepsilon}$ stand for stress, strain and strain rate, respectively, and $i = 1, 2$ while $j = i + 1$. Table 3 summarizes the various parameters and

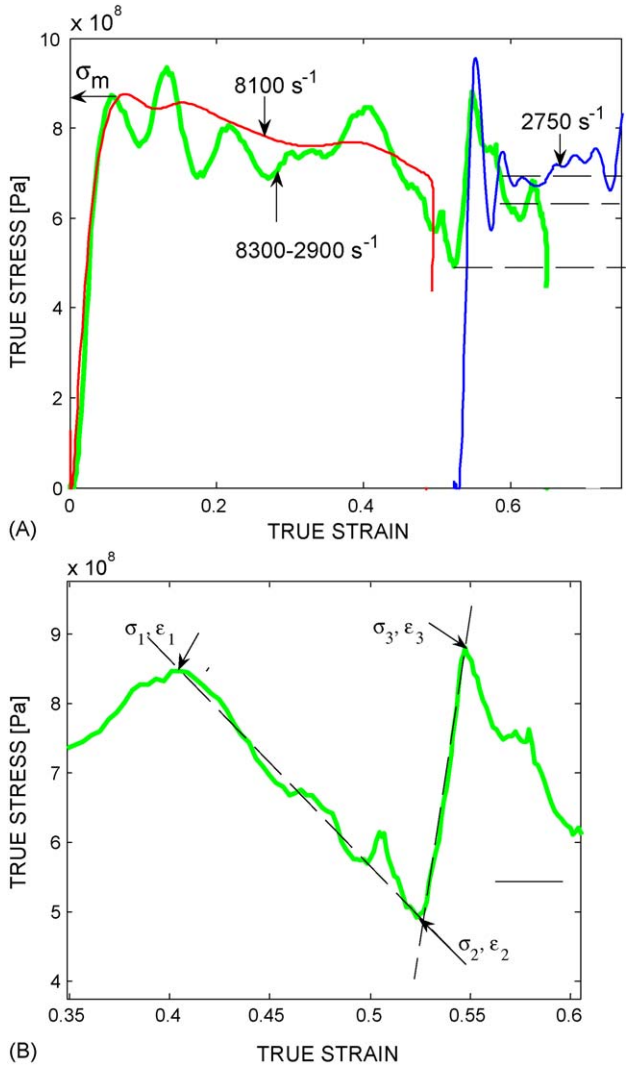

Fig. 7. (A) Typical true stress–strain curve obtained for a strain-rate jump test. Note the transient behavior resulting from the jump. Curves obtained from monotonous tests have been superimposed to illustrate the steady state response. In these tests, σ_M is the maximum stress level reached during the test. (B) Magnified view of the transient section of the stress–strain curve during a typical jump tests.

results of the strain-rate jump tests. Since each test was carried out at a different range of strain rates and therefore different transitional strains, the following parameters are defined to establish a comparative basis: M_{12} and M_{23}: the unloading and loading and moduli, σ_M: the maximum stress reached during the test (at the onset of plastic flow–Fig. 7A), ε_1 and ε_2: the strains at which unloading started and reached the next stable state (Figs. 7A and B), and $W(\varepsilon_1) = \int_0^{\varepsilon_1} \sigma de$: the strain energy invested up to unloading strain ε_1. Fig. 8 is a plot of M_{12} (unloading) as a function of W. This figure indicates a possible correlation between these parameters, in the sense that M_{12} decreases as W increases, to reach some constant value at $W \approx 2.5 \times 10^8\ J/m^3$. Fig. 9 is a plot of M_{12} and M_{23} as a function of σ_M. From this plot, both slopes are relatively similar and well correlated to σ_M. The plot shows an inflexion point at $\sigma_M \approx 850\ MPa$. It should be noted that this stress level is reached at $\dot{\varepsilon} \approx 8000\ s^{-1}$ (Fig. 9). As a

Table 3
Summary of parameters for strain-rate jump tests: w and t are the width and thickness of the gauge, respectively, ε_1 and ε_2 are the strains at which unloading starts and stabilizes with corresponding strain rates $\dot{\varepsilon}_1$ and $\dot{\varepsilon}_2$, M_{12} and M_{23} are hardening moduli, and W is the strain energy up to ε_1

SPEC	w (mm)	t (mm)	$\dot{\varepsilon}_1 \rightarrow \dot{\varepsilon}_2$ (s^{-1})	$\varepsilon_1 \rightarrow \varepsilon_2$	M_{12} (GPa)	M_{23} (GPa)	$W(\varepsilon_1)$ (J/m^3)
AL2	2.55	2.50	2800–1300	0.15-0.18	81.9	80	7.8e7
AL3	2.55	2.50	4500–2900	0.24-0.27	33.7	38.4	1.5e8
AL4	2.55	2.50	6000–2000	0.33–0.38	34.1	32.5	2.22e8
AM1	1.65	2.61	8300–2900	0.42–0.51	3.0	16.3	3.05e8
AM2	1.65	2.55	6700–2200	0.34–0.41	16.4	7.2	2.46e8
AM3	1.65	2.51	7600–2700	0.4–0.48	9.14	14.7	2.43e8
AM4	1.65	2.57	6800–3700	0.19–0.24	3.0	14.3	1.55e8
AM6	1.65	2.60	2.8e–2–4e–4	0.11	144	225	3.05e7
AS1	0.6	2.50	13000–4300	0.67–0.82	6.9	7.0	4.5e8
AS2	0.6	2.50	5500–9000	0.29–0.42	3.1	1.5	1.65e8
AS4	0.6	2.42	13700–5000	0.62–0.83	3.2	12.6	4.62e8
AS5	0.6	2.35	14500–8000	0.42–0.51	4.0	5.5	3.10e8

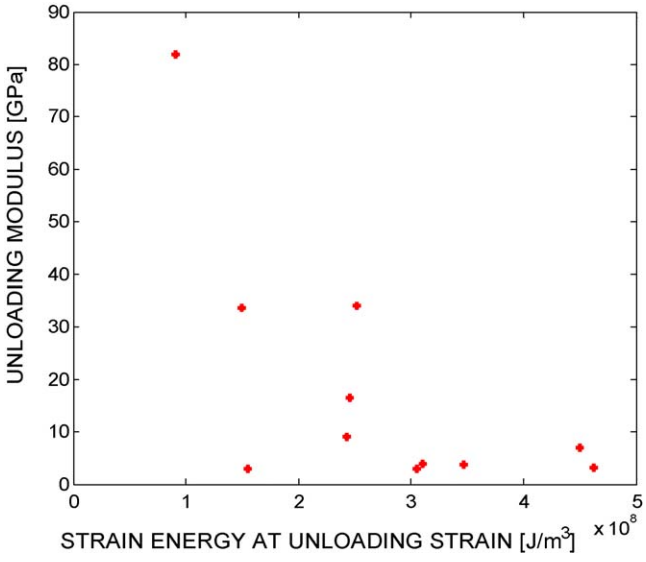

Fig. 8. Plot of the unloading modulus M_{12} as a function of the strain energy $W(\varepsilon_1)$.

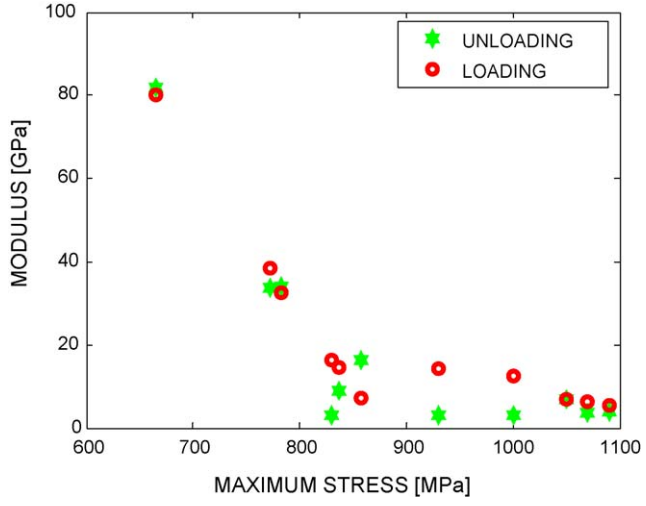

Fig. 9. Plot of the moduli M_{12} and M_{23} as a function of σ_M (Fig. 7A).

reminder, the materials exhibit noticeable softening at this strain rate (Fig. 2).

3.2. Microstructural characterization

3.2.1. Optical metallography

Fig. 10 describes the evolution of the microstructure at the center of the gauge section, as taken from polished mid-section specimens. The initially equiaxed grains tend to align with the shear direction, and develop an increasingly oblong shape to the point where individual grains are no longer discernable at $\dot{\varepsilon} = 11500\,s^{-1}$. As the strain rate increases, the microstructure gets darker upon etching (the various grades of etching of the grains do not bear any significance in terms of strain or crystallography, as observed in [11]). It is also noted that for all strain rates, relatively few twins or Neumann bands were observed as long as the individual grain remains discernable. The microstructures shown in Fig. 10 should be contrasted with those obtained after hydrodynamic shock loading, since the present specimens undergo extensive shear as opposed to almost purely elastic deformation (see e.g. [11]). Therefore, the present grains do not retain their initial shape. By contrast, it is interesting to compare the present microstructures with those resulting from ballistic impact at several km/s, for which both shear and pressure loading develop as well as high temperatures [19].

Finally, it is important to mention that none of the specimens investigated by optical methods disclose any sign of shear localization (e.g. such as adiabatic shear bands) or apparent damage mechanism. This observation is all the more important that shear localization is well known to cause a macroscopic strain-softening response.

3.2.2. Transmission electron microscopy (TEM)

Typical microstructures observed by TEM are shown in Fig. 11. The undeformed material has the typical microstructure of annealed Fe, namely equiaxed grains and very low dislocation density (Fig. 11A). Quasi-static deformation ($\varepsilon = 2$; $\dot{\varepsilon} \approx 10^{-3}\,s^{-1}$) results in the formation of dislocation cells, while the original grain size is preserved (Fig. 11B). At higher strain rate ($\varepsilon = 0.3$; $\dot{\varepsilon} \approx 10^{3}\,s^{-1}$) the microstructure is quite het-

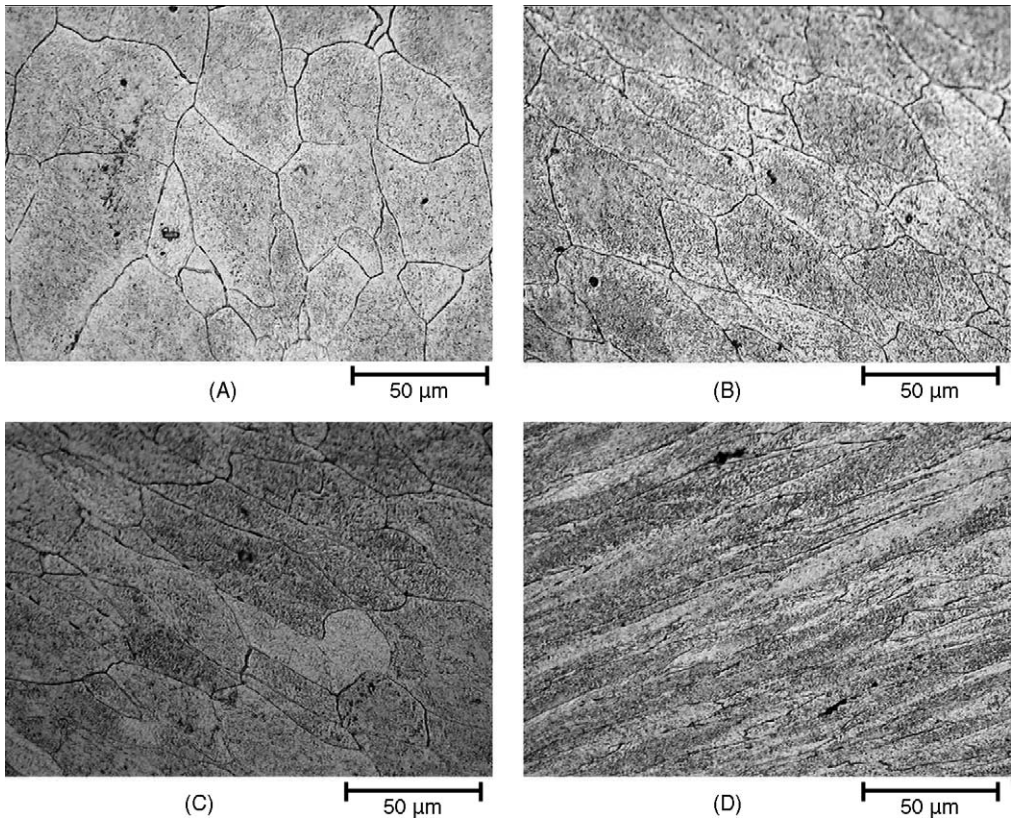

Fig. 10. Typical microstructures of the investigated Fe. Nital ecthant (3%). (A) Undeformed material, (B) $\varepsilon = 0.40$; $\dot{\varepsilon} = 3500\,s^{-1}$, (C) $\varepsilon = 0.38$; $\dot{\varepsilon} = 6300\,s^{-1}$, and (D) $\varepsilon = 1.4$; $\dot{\varepsilon} = 11500\,s^{-1}$.

erogeneous, consisting of micro-twins, large twins and a few dislocation cells (Fig. 11C). By contrast, the very high-rate ($\varepsilon = 0.7$; $\dot{\varepsilon} \approx 10^4\,s^{-1}$) microstructure is more homogeneous, comprising micro-twins and 200 nm dynamically recrystallized grains (Fig. 11D). At this stage, the original microstructure has undergone considerable refinement. Identification of the remaining microstructure has long been known to be a delicate point as the phase transformation is fully reversible. While twinning has been addressed in the introductory section, it should be mentioned that marked microstructural refinement occurs when the shock pressure exceeds 13 GPa [17]. Leslie et al. [16] attribute the difficulty in identification of the residual microstructure to the fact that the phase transition is incomplete until a pressure of 23 GPa is reached, thus causing the coexistence of transformed and untransformed phases. These authors also claim that at higher pressures, the adiabatic heating effects responsible for recrystallization may erase any specific signs of a former transformation. The results shown here indicate first of all a noticeable microstructural refinement with clear evidence of dynamic recrystallization.

3.3. In situ temperature measurement

Fig. 12A shows a representative stress–strain and temperature–strain relationship for a representative high strain-rate experiment ($\dot{\varepsilon} \approx 8400\,s^{-1}$). While this measurement provides an averaged temperature value, it nevertheless gives a valuable indication of the evolution of the temperature in this nearly adiabatic process. The "efficiency" of the thermomechanical conversion can be assessed by defining $\beta_{int} = \frac{\Delta E_T}{\Delta E_M}$ [39]. This coefficient characterizes the ratio of thermal to mechanical energy. One would naturally expect from thermodynamic considerations that $\beta_{int} \leq 1$ if no additional heat input, other than that due to the deformation process, is generated. Fig. 12B shows the evolution of β_{int} at a lower ($\dot{\varepsilon} = 3800\,s^{-1}$) and a higher ($\dot{\varepsilon} = 8400\,s^{-1}$) strain rate. A very surprising, yet consistently repeatable result is that for the high strain-rate experiments, $\beta_{int} \geq 1$ which can be meaningful if an internal heat source other than plastic dissipation assumed. One should note that at this strain rate ($\dot{\varepsilon} = 8400\,s^{-1}$), the material is observed to strongly strain soften (Fig. 4). In addition, this strain rate belongs to the range of strain rates where M_{12} and M_{23} reach minimal values (Fig. 9).

4. Discussion

This study addresses the mechanical response of pure iron subjected to dominant shear loading over a large range of strain rates. As mentioned throughout the paper, many studies of the dynamic response of iron have been made over the years, with the emphasis being either on dynamic uniaxial compression, torsion to a much lesser extent, and on shock loading. While the first type of study addressed mostly the mechanical response and to some extent the underlying microstructure, the second type of studies have essentially emphasized various aspects of the reversible α (BCC) $\Leftrightarrow$ ε (HCP) phase transition, as well as some microstructural aspects.

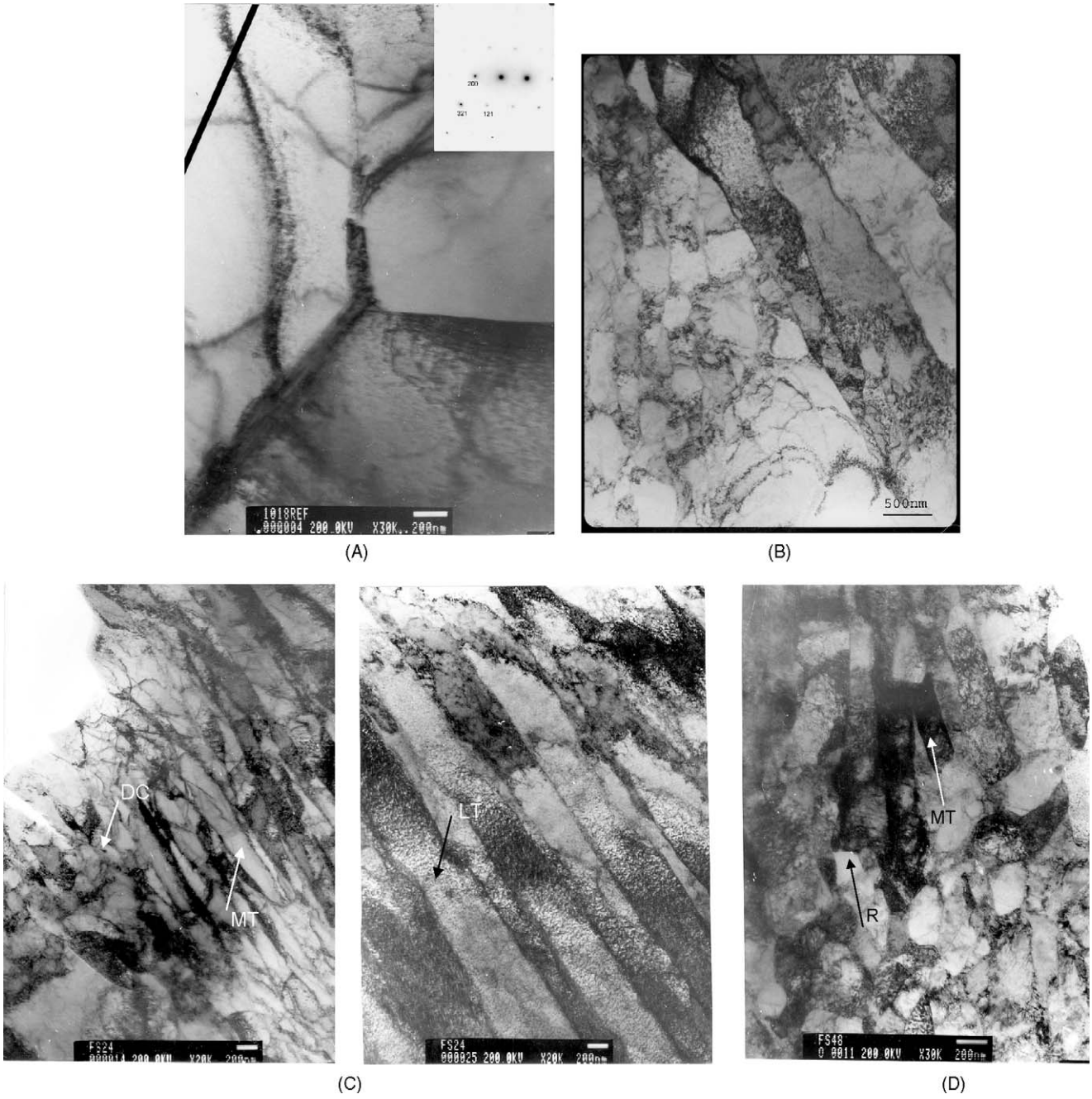

Fig. 11. Typical microstructure of pure iron. Transmisson electron microscopy. (A) Undeformed material, (B) quasi-static rate of $\varepsilon = 2$; $\dot{\varepsilon} \approx 10^{-3}\ \mathrm{s}^{-1}$. Dislocation cells structure, (C) $\varepsilon = 0.3$; $\dot{\varepsilon} \approx 10^{3}\ \mathrm{s}^{-1}$. Micro-twins (MT), dislocation cells (DC) and large twins (LT). Both pictures taken at the same magnification at different areas. Note the heterogeneous microstructure, (D) $\varepsilon = 0.7$; $\dot{\varepsilon} \approx 10^{4}\ \mathrm{s}^{-1}$. Micro-twins (MT) and recrystallized grains (R).

However, there is little if no overlap between the two types of studies, as the issue of a potential phase transformation has always appeared to require stress levels that greatly exceed those achieved during dynamic uniaxial compression. One noticeable exception is found in the work of Weston [4] who pointed out the influence of a prior transformation (preshocked to 40 GPa) on the subsequent high strain-rate properties of pure Fe. The present work addresses the mechanical behavior of this material under dominant shear conditions, using a single specimen geometry in a seamless manner over a wide range of strain rates. Various experimental techniques have been used throughout this work, ranging from macroscopic mechanical behavior to detailed microstructural description in order to address various aspects of many outstanding issues. Several interesting results have emerged from this work that must be understood, as discussed next.

The optical and TEM characterization indicates that the starting material is *annealed* as evidenced by the large equiaxed grains with a very low dislocation density. This observation stands immediately at odds with the results of the mechanical

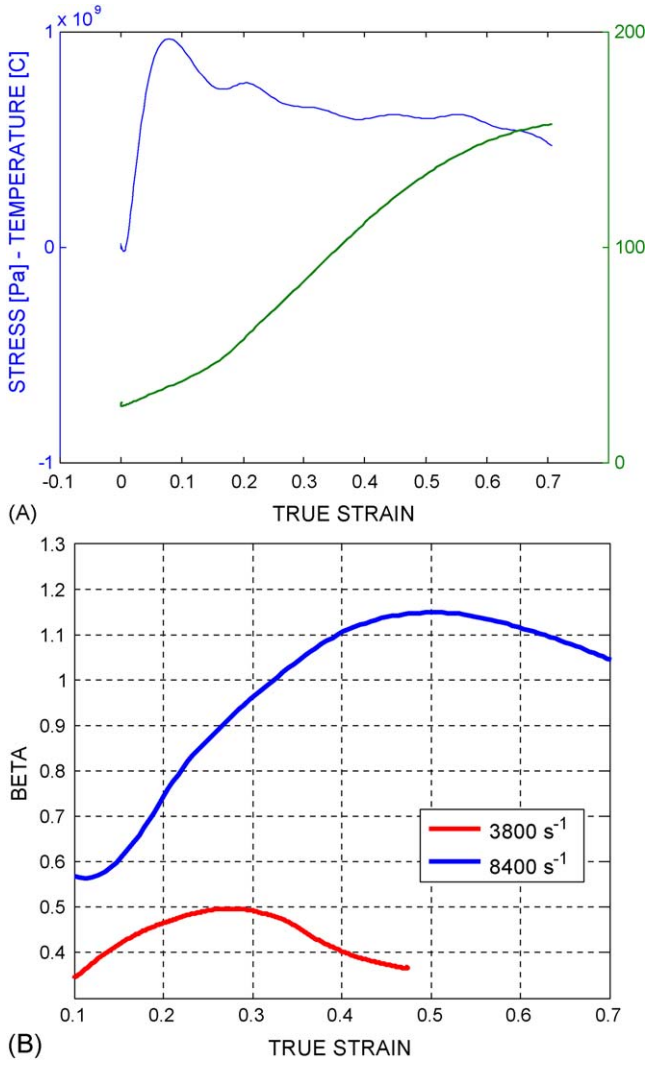

Fig. 12. (A) Typical true stress–strain–temperature record. $\dot{\varepsilon} = 8400\,s^{-1}$. (B) Plot of b factors as a function of strain at two strain rates. Note that $\beta \geq 1$ at $\dot{\varepsilon} = 8400\,s^{-1}$.

tests. While the rate sensitivity of our material is that classically observed, Figs. 2 and 4 show that, at relatively high strain rates of the order of $\dot{\varepsilon} \approx 8000\,s^{-1}$ and above, significant strain softening develops *from the very onset of plastic flow*. This behavior is unexpected for the annealed material while it fits exactly that of a similar iron *preshocked* (40 GPa) beyond the phase transformation threshold (≈13 GPa). Here, the preshocking treatment must be related to the residual microstructure that results from the phase transformation. Strain softening cannot be attributed to thermal softening, as a result of adiabatic heating, since the latter is well known and shown to be insignificant at small plastic strains. Another potential factor for strain softening is that of the material instability caused by shear localization, adiabatic shear bands in this case. However, such bands were not observed, in accord with previous researchers [6]. The TEM study failed to reveal any trace of residual HCP phase, as expected from the reversible nature of the phenomenon. However, the evolution of the microstructure at various strains and strain rates was characterized and a global refinement of the structure was observed with increase of strain rate (coarse twins to dislocation cells to fine twins and recrystallized grains).

Another interesting observation is that of dynamic recrystallization. This phenomenon has been reported to develop in various impact configurations, including ballistic impacts that generate pressures in excess of the transformation pressure. Dynamic recrystallization is generally reported to occur after the phase transformation (see e.g. [19,21,40]). However, some uncertainty remains as to this phenomenon. While Murr and Esquivel [19] report dynamic recrystallization following impact loading at several km/s, Johnson et al. [40] showed a very fine apparently recrystallized structure which they attribute to the inverse phase transformation only, based on their observation that the kinetics of recrystallization require a long time. It should again be emphasized that in the latter shock loading experiment, plastic deformation is minimal as opposed to the experiments reported here. It is interesting to note that fine recrystallized grains are identified to be part of adiabatic shear bands [19] that might contribute to the overall strain-softening behavior, provided they formed at the onset of plastic flow in the present case. While this eventuality does not seem likely, one could speculate that the formation of a fine-grained second (transformed) phase at σ_M might have the same destabilizing effect on the mechanical response. The temperature measurements showed an abnormal behavior, at the higher strain rates only. Namely, to justify the fact that $\beta_{int} \geq 1$, one can either invoke an experimental error, or assume the operation of an extra heat source in addition to the thermomechanical conversion of plastic work into heat. The very same equipment and experimental procedures has been used in previous measurements for other metals [37], yielding credible and repeatable results, so that the experimental error is not very likely. However, to verify the present results, a series of HSLA100 steel specimens were tested in identical conditions and for none of them did one observe that $\beta_{int} \geq 1$. On the other hand, recrystallization of Fe is exothermic [41], and while there are no reported measurements of the heat released during dynamic recrystallization in particular, the present results suggest that the additional heat source is indeed linked the dynamic recrystallization that was observed in the TEM characterization.

The hardness of the deformed material reaches values in excess of 250 HVN for the high strain rates. While such values are often associated with a post-shock state, it was observed that hardness is an ambiguous indicator here when large plastic deformations are involved. Specifically, large strain quasi-static deformation can yield very high hardness values as well (Fig. 5).

Jump tests revealed a well-structured response of the stress to the sudden change of strain rate, similar to results reported in [38] for an austenitic stainless steel. Two slopes are characterizing this response, corresponding to unloading and loading, respectively. As the jump requires a finite time (thus strain increment) to complete, one does not probe a "frozen" microstructure, but rather an evolving one. The exact physical mechanism that dictates the response has not been the subject of this study nor has it been characterized. Yet, among various possible correlations, it appears that the most instructive one is that shown in Fig. 9 where the strain-hardening moduli (unloading/loading

slopes) are correlated to the maximum stress. In fact, comparing Fig. 8 with Fig. 9, it appears that the maximum stress σ_M is much better correlated to the moduli than the accumulated strain energy. While a rational explanation for this observation is not evident, one should nevertheless note that the transition occurs at $\sigma \approx 850$ MPa corresponding to $\dot{\varepsilon} \approx 8000\,s^{-1}$.

One can now summarize all the experimental findings as follows: the unique high strain-rate softening behavior strongly suggests that a critical stress ($\sigma \approx 850$ MPa) triggered α (BCC) $\Leftrightarrow \varepsilon$ (HCP) phase transformation is taking place at strain rates of the order of ($\dot{\varepsilon} = 8400\,s^{-1}$). This complements the experiments of Weston [4] in which a two phase process (hydrodynamic preshock at 40 GPa followed by reloading) was applied, whereas a single stage uniaxial shear compression loading was applied here and observed to yield identical results. Weston [4] attributed the softening behavior to the previous phase transformation that preceded the impact test. Analogous reasoning leads to the conclusion that the present observation of strain softening at high rates is of a similar nature. The phase transformation is followed by later dynamic recrystallization that is an exothermal phenomenon ($\beta_{int} \geq 1$, Fig. 12B) recorded by infrared sensing. While the reversible character of the phase transformation makes it difficult to assess *a posteriori* (e.g. by TEM), as repeatedly pointed out in the literature, the potential role of shear deformation has been recently emphasized [30,42], and the present experiments support this suggestion. Therefore, it appears that two important factors ought to be taken into account: the high-rate sensitivity of pure Fe and the shear dominant nature of the reported experiments.

Future work should concentrate of the characterization of the phase transformation in real time, using e.g. *in situ* high-speed X-ray diffraction. Similarly, other metallic systems that possess a stable pressure induced phase transformation should be investigated using the present SCS technique for high-rate shear loading.

5. Conclusions

- The present work has presented new results on the dynamic mechanical behavior of pure Fe subjected to dominant shear loading that was largely unexplored so far.
- A high strain-rate sensitivity was observed, resulting in high strain-rate strength levels that are comparable to the strength of alloyed steels.
- For strain rates of the order of $8000\,s^{-1}$, pure Fe exhibits significant strain softening behavior from the onset of plastic flow.
- This observation contradicts the microstructural observation of an annealed initial condition which is reported to retain strain-hardening capacity at high strain rates.
- Identical high strain-rate strain softening and flow behavior was reported for Fe specimens that had been previously preshocked to 40 GPa, thus above the critical α (BCC) $\Leftrightarrow \varepsilon$ (HCP) transformation [4].
- Noticeable microstructural refinement was observed as the strain rate increases, ultimately yielding a new recrystallized microstructure.
- Dynamic recrystallization was identified as the external heat source causing an abnormal thermal behavior recorded during the impact experiments.
- The $\alpha \Leftrightarrow \varepsilon$ phase transformation cannot be dissociated from the present context and appears to be responsible for the observed softening behavior at high strain rates and subsequent recrystallization.
- The observed strain softening behavior is at full agreement with Weston's [4] observations and claim that the $\alpha \Leftrightarrow \varepsilon$ phase transition is causing it.
- The $\alpha \Leftrightarrow \varepsilon$ phase transformation is tentatively identified to develop when a peak stress of $\sigma \approx 850$ MPa is attained at strain rates of the order of $\dot{\varepsilon} \approx 8000\,s^{-1}$ under dominant shear loading.
- The present experiments support recent reports about the role of shear deformation in promoting allotropic phase transitions [30].
- Additional work should concentrate on *in situ* X-ray characterization of the phase transformation using the present SCS technique.

Acknowledgements

The research reported here was supported by the US Department of Energy through the ASCI Alliance Center for Simulation of Dynamic Response of Materials at the California Institute of Technology and is gratefully acknowledged. Professors T.J. Ahrens, K. Bhattacharya and G. de Botton are gratefully acknowledged for the stimulating discussions. We acknowledge M. Tao and S. Mizrachi for their technical assistance. DR acknowledges support of the Fund for Promotion of Research at Technion. GR acknowledges the support of the Office of Naval Research (Dr. J.A. Christodoulou, Program Manager) for his research on dynamic behavior of metals.

References

[1] J. Klepaczko, Int. J. Solids Struct. 5 (1969) 533.
[2] H. Watson Jr., Int. J. Solids Struct. 6 (1970) 1157.
[3] P.S. Follansbee, Proc. Inst. Phys. Conf. Ser. 102 (1989) 213.
[4] G.M. Weston, J. Mater. Sci. Lett. 11 (1992) 1361.
[5] D. Ostwaldt, J.R. Klepaczko, P. Klimanek, J. Phys. IV France Colloq. C3 (7) (1997) 385.
[6] C. Mason, M.J. Worswick, Int. J. Fract. 111 (2001) 29.
[7] D. Jia, K.T. Ramesh, E. Ma, Scripta Mater. 42 (2000) 73.
[8] C. Nicolazo, M. Leroy, Mech. Mater. 34 (2002) 231.
[9] A.T. Churchman, A.H. Cottrell, Nature 167 (1951) 943.
[10] A. Kelly, Proc. Phys. Soc. 70 (1952) 403.
[11] C.S. Smith, Trans. AIME (1958) 574.
[12] G.E. Dieter, Strengthening Mechanisms in Solids, ASM Metals Park, OH, 1960, p. 279.
[13] E. Bull, Simonsen, Acta Met. 8 (1960) 809.
[14] E. Hornbogen, TMS-AIME 221 (1961) 711.
[15] A.R. Rosenfield, B.L. Averbach, M. Cohen, Acta Met. 11 (1963) 1100.
[16] W.C. Leslie, D.W. Stevens, M. Cohen, in: V.F. Zackay (Ed.), High Strength Materials, John Wiley & Sons, NY, New York, 1965, p. 382.
[17] S. Mahajan, Phil. Mag. 19 (1969) 199.
[18] J.N. Johnson, R.W. Rohde, J. Appl. Phys. 42 (11) (1971) 4171.
[19] L.E. Murr, E.V. Esquivel, J. Mater. Sci. 39 (2004) 1153.
[20] Z. Rosenberg, Y. Partom, D. Yaziv, J. Phys. D.: Appl. Phys. 13 (1980) 1489.

[21] K. Dan, H. Tamura, A.B. Sawaoka, T. Mori, Jpn. J. Appl. Phys. 33 (1994) 2667.
[22] D. Bancroft, E.L. Peterson, S.J. Minshall, J. Appl. Phys. 27 (1956) 291.
[23] Y. Horie, G.E. Duvall, Behaviour of Dense Media under High Dynamic Pressure, Gordon and Breach, New York, 1965, p. 355.
[24] L.M. Barker, R.E. Hollenbach, J. Appl. Phys. 45 (1974) 4872.
[25] T.J. Ahrens, K.G. Holland, G.Q. Chen, Geophys. Res. Lett. 29 (7) (2002) (Art. no. 1150).
[26] J.C.F. Millett, N.K. Bourne, Z. Rosenberg, J. Appl. Phys. 816 (1997) 2579.
[27] T. Sano, H. Mori, E. Ohmura, I. Myamoto, Appl. Phys. Lett. 83 (17) (2003) 3498.
[28] O.E. Jones, R.A. Graham, Accurate Characterization of the High Pressure Environment, NBS Special Publication 326, Gaithersburg MD, 1968, p. 229.
[29] N. Von Bargen, R. Boehler, High Press. Res. 6 (1990) 133.
[30] K.J. Caspersen, A. Lew, M. Ortiz, E.A. Carter, Phys. Rev. Lett. (2004) 115501.
[31] A. Laio, S. Bernard, G.L. Chiarotti, S. Scandolo, E. Tosatti, Science 287 (2000) 1026.
[32] A.B. Belonoshko, R. Ahuja, B. Johansson, Nature 424 (2003) 1031.
[33] D. Rittel, S. Lee, G. Ravichandran, Exp. Mech. 42 (1) (2002) 58.
[34] M. Vural, D. Rittel, G. Ravichandran, Metall. Trans. 34A (12) (2003) 2873.
[35] H. Kolsky, J. Phys. Soc. Lond. 62-B (1949) 676.
[36] J.M. Lifshitz, H. Leber, Int. J. Impact Eng. 156 (1994) 723.
[37] J. Hodowany, G. Ravichandran, A.J. Rosakis, P. Rosakis, Exp. Mech. 40 (2) (2000) 113.
[38] S. Venkadesan, P. Rodriguez, K.A. Padmanabhan, P.V. Sivaprasad, C. Phaniraj, Mater. Sci. Eng. A 154 (1) (1992) 69.
[39] G.I. Taylor, H. Quinney, Proc. R. Soc. A 143 (1934) 307.
[40] P.C. Johnson, B.A. Stein, R.S. Davis, J. Appl. Phys. 33 (1962) 557.
[41] F. Scholz, E. Woldt, J. Therm. Anal. Calorim. 64 (2001) 895.
[42] A. Lew, K.J. Caspersen, E.A. Carter, M. Ortiz, J. Mech. Solids Phys. 546 (2006) 1276.